

Diagnostic algorithm for glioma grading using dynamic susceptibility contrast-enhanced magnetic resonance perfusion and proton magnetic resonance spectroscopy

DINH HIEU NGUYEN^{1,2*}, DUY HUNG NGUYEN^{1,3*}, THANH DUNG LE^{3,4},
HA KHUONG NGUYEN¹, VAN ANH NGUYEN-THI⁵ and MINH DUC NGUYEN⁶

¹Department of Radiology, Hanoi Medical University; ²Department of Radiology, Ha Dong General Hospital;
³Department of Radiology, Viet Duc Hospital; ⁴Department of Radiology, VNU University of Medicine and Pharmacy,
Vietnam National University; ⁵Department of Radiology, Hanoi Medical University Hospital, Hanoi 100000;
⁶Department of Radiology, Pham Ngoc Thach University of Medicine, Ho Chi Minh City 700000, Vietnam

Received July 17, 2023; Accepted December 14, 2023

DOI: 10.3892/br.2024.1741

Abstract. The present retrospective study aimed to investigate the diagnostic capacity of and design a diagnostic algorithm for dynamic susceptibility contrast-enhanced MRI (DSCE-MRI) and proton magnetic resonance spectroscopy (¹H-MRS) in grading low-grade glioma (LGG) and high-grade glioma (HGG). This retrospective study enrolled 57 patients, of which 14 had LGG and 43 had HGG, five had World Health Organization grade 1, nine had grade 2, 20 had grade 3 and 23 had grade 4 glioma. All subjects underwent a standard 3T MRI brain tumor protocol with conventional MRI (cMRI) and advanced techniques, including DSCE-MRI and ¹H-MRS. The associations of grade categorization with parameters in tumor and peritumor regions in the DSCE-MRI were examined, including tumor relative cerebral blood volume (TrCBV) and peripheral relative (Pr)CBV, as well as Tr and Pr cerebral blood flow (CBF) and ¹H-MRS, including the creatine (Cr) and N-acetyl aspartate (NAA) ratios of choline (Cho), i.e. the TCho/NAA, PCho/NAA, TCho/Cr and PCho/Cr metabolite ratios. The data were compared using the Mann-Whitney U-test, independent samples t-test, Chi-square test, Fisher's exact test and receiver operating characteristic curve analyses. Decision tree analysis established an algorithm based on cutoffs for specified significant parameters. The PrCBF had

the highest performance in the preoperative prediction of histological glioma grading, followed by the TrCBV, PrCBF, TrCBV, PCho/NAA, PCho/Cr, TCho/NAA and TCho/Cr. An algorithm based on TrCBV, PrCBF and TCho/Cr had a diagnostic accuracy of 100% for LGG and 90.7% for HGG and a misclassification risk of 7%. The cutoffs (sensitivity and specificity) were 2.48 (86 and 100%) for TrCBV, 1.26 (83.7 and 100%) for PrCBF and 3.18 (69.8 and 78.6%) for TCho/Cr. In conclusion, the diagnostic algorithm using TrCBV, PrCBF and TCho/Cr values, which were obtained from DSCE-MRI and ¹H-MRS, increased diagnostic accuracy to 100% for LGGs and 90.7% for HGGs compared to previous studies using conventional MRI. This non-invasive advanced MRI diagnostic algorithm is recommended for clinical application for constructing preoperative strategies and prognosis of patients with glioma.

Introduction

Gliomas are one the most frequent primary brain neoplasm and are categorized into four grades with increasing malignancy, as low-grade glioma (LGG; grades 1 and 2) and high-grade glioma (HGG; grades 3 and 4), based on the histopathological standard of the World Health Organization (WHO) classification for the central nervous system (1). Gliomas are heterogeneous and vary significantly in terms of various histopathological features, clinical symptoms, imaging features and prognoses (2-4). The grading of gliomas has a crucial role in constructing an appropriate treatment strategy and predicting survival (2-10).

Magnetic resonance imaging (MRI) has been universally used as a non-invasive method for diagnosing and grading intracranial neoplasms, particularly in gliomas. Despite its popularity and evaluability, several previous studies have shown that conventional MRI (cMRI) sensitivity and specificity fluctuate around 72.5 and 65.0%, respectively (6). In addition, cMRI has certain limitations in grading tumors, since their degree of enhancement may be associated with the angiogenesis of the tumor or the breakdown of the

Correspondence to: Dr Minh Duc Nguyen, Department of Radiology, Pham Ngoc Thach University of Medicine, 2 Duong Quang Trung Ward 12 District 10, Ho Chi Minh City 700000, Vietnam
E-mail: bsnguyenminhduc@pnt.edu.vn

*Contributed equally

Key words: dynamic susceptibility contrast-enhanced MRI, proton magnetic resonance spectroscopy, high-grade glioma, low-grade glioma, WHO grading

blood-brain barrier. In addition, certain HGGs may show little or no enhancement (estimated to be up to 40%) (7), while certain LGGs may show prominent enhancement (6,9). HGGs are characterized by infiltration into the brain parenchyma along vascular channels and white matter fibers surrounding the tumor (also called the peritumoral region). These peritumoral regions may be inappropriately analyzed without signal abnormalities or enhancement, even misdiagnosed on cMRI as either peritumoral edema or normal parenchyma. Furthermore, cMRI is limited in providing reliable information on tumor physiology, such as microvascular proliferation, metabolism, micro-necrosis or cell density (6,11).

These limitations may be addressed using a multi-modal approach, utilizing several advanced MRI techniques, including dynamic susceptibility contrast-enhanced MRI (DSCE-MRI), proton magnetic resonance spectroscopy (¹H-MRS), diffusion-weighted imaging (DWI) and diffusion tensor imaging (DTI), to provide a comprehensive evaluation of different aspects of glioma characteristics (6,8-10,12). Advanced MRI combining DSCE-MRI and ¹H-MRS has become most frequently practical for assessing tumor angiogenesis and metabolism, which are strongly associated with glioma malignancy (2-4,6-8,12). DSCE-MRI provides valuable information on the histophysiology, particularly in the vascularity and angiogenesis in tumors, a process often associated with higher-grade gliomas, and gives insight into the blood flow dynamics of tumors (7,11,12). ¹H-MRS presents the metabolic profile of tumor and peritumor regions based on specific metabolite ratios; this is valuable for understanding the biochemistry of the tumor (8,9,13). These two most common advanced MRI techniques are commonly used on 1.5 and 3.0 Tesla MRI machines for diagnosis and to complement the imaging features of cMRI and aid in making an accurate diagnosis, particularly for grading glioma, as they offer a more holistic view of the glioma's characteristics. The accuracy rate of glioma grading before and after adding MRS image assessment in the study by Shakir *et al* (14) was 69 and 88%, respectively. Meanwhile, DTI and DWI primarily capture the movement of water molecules within tissues that rely on the principle of free Brownian motion of water molecules, reflecting aspects such as cellularity and tissue architecture (15-17). This can offer valuable insight into cellular density, organization and the integrity of white matter tracts within the normal brain tissue and the tumoral regions, which are particularly sensitive to cellular changes, as high-grade gliomas often exhibit increased cell density, leading to restricted water diffusion. However, they do not directly measure the metabolic characteristics composition due to intra-tumoral pathological changes or perfusion-related dynamics details as in the case of ¹H-MRS and DSCE-MRI, respectively. A study by Law *et al* (6) using 1.5T MRI showed that the combination of parameters obtained from ¹H-MRS and DSCE-MRI, including the relative cerebral blood volume-(CBV) ratio of the tumor to normal white matter (NWM)-(rCBV) and tumoral choline (Cho)/creatine (Cr) and Cho/N-acetyl aspartate (NAA) ratios, increased the sensitivity of grading glioma to 93.3% compared to cMRI (72.5%), with a specificity of 60 and 65%, respectively. A study by Hasan *et al* (13) indicated that combining Cho/NAA and rCBV increased diagnostic

accuracy to 100%. To our knowledge, no previously published study has evaluated and developed an algorithm for grading glioma using DSCE-MRI and ¹H-MRS parameters on a 3T MRI system, which has a crucial role in treatment planning, surgical strategy and predicting patients' overall prognosis and survival. Furthermore, even if various studies had been carried out, there was no specific consensus on thresholds, and imaging-based algorithms for the perfusion and spectroscopy parameters were developed to determine cutoffs for glioma classification (13,14,18). Therefore, the present study aimed to determine the diagnostic value and establish an imaging-based algorithm for differentiating between HGG and LGG using DSCE-MRI and ¹H-MRS parameters on 3T MRI.

Patients and methods

Study population. All patients in this retrospective study were recruited at Viet Duc University Hospital (Hanoi, Vietnam) and the study was conducted at the Department of Radiology of Viet Duc University Hospital between June 2021 and March 2022. The study population was collected using a consecutive sampling method attributable to the lack of a previous algorithm to estimate the minimum sample size required. Data were collected from all of the patients who met the selection criteria and did not meet the exclusion criteria during the study period.

The selection criteria were as follows: i) The research subjects were examined with a 3T MRI scanning system (SIGNA Pioneer MR; GE Healthcare) with the same protocol comprising cMRI, DSCE-MRI and ¹H-MRS (Table I); ii) these patients underwent surgery or stereotactic biopsy after MRI examination with the pathological result of LGG or HGG.

The exclusion criteria were as follows: i) Patients with a previous history of biopsy or treatment, such as cranial radiotherapy and operative resection of the tumor; and ii) apparent motion or any artifacts affecting the quality of MRI images that prevent accurate measurements were also eliminated from this study.

The present study was approved by Hanoi Medical University's Institutional Review Board (Hanoi, Vietnam; ref. no. 827/GCN-HDDDNCYSH-DHYHN; dated 03/28/2023) and was performed according to the Declaration of Helsinki (revised in 2013). Since this study was retrospective, the requirement for informed consent from adult patients, pediatric patients and their parents/guardians to participate in the research (including patient personal information and imaging data characteristics) was waived.

MRI technique. The patients underwent MRI brain examinations using a 3T scan system with a head coil. The same technique statistics and protocol were applied to all patients (Table I). General anesthesia may be indicated due to prolonged examinations, particularly in children aged <6 years or patients with altered mental status conditions. This specific indication was solely assessed in every single case. Informed consent from the patient or their guardians/parents for general anesthesia and contrast enhancement material injection was documented in the patient's medical health record. DSCE-MRI was obtained before T1-weighted (T1W) contrast enhancement MRI.

Table I. Imaging protocol.

Sequence	Plane	TR, msec	TE, msec	Thickness, mm	Matrix	FOV
T2*	Axial	200	10	5	256x256	240x240
T2W TSE	Axial, coronal	2500	100	5	360x288	240x240
T1W	Axial, sagittal	2325	24	5	256x256	300x224
T1W CE+ ^a	Axial, sagittal	2325	24	5	256x256	300x224
DSCE-MRI ^b	GRE EPI	1250	45	5	88x87	338x240
¹ H-MRS ^c	2D multivoxel CSI	8500	117	-	-	240x240

^aT1W, T1W spin echo; CE+, a single dose of intravenous contrast agent injection (with an injection rate of 5 ml/sec, gadolinium-DTPA-0.1 ml/kg); ^bDSCE-MRI was performed using dynamic T2*-weighted GRE EPI; intravenous injection of contrast agent (gadolinium-DTPA, with an injection rate of 5 ml/sec, 0.1 ml/kg); 40 scans; acquisition voxel size 2.5x2.5x5 mm. DSCE was performed before T1 SE CE+ during the first pass of a bolus intravenous contrast injection. TR, repetition time; TE, echo time; FOV, field of view; DSCE, dynamic susceptibility contrast-enhanced; T2*, T2 gradient echo sequence; T2W TSE, T2-weighted turbo spin-echo; GRE EPI, gradient-recalled echo-planar imaging; FOV, field of view; CSI, chemical shift imaging; ¹H-MRS, proton magnetic resonance spectroscopy.

Image analysis. MRI images were reinterpreted by a radiologist (using the workstation of AW VolumeShare 7 system; GE Healthcare) with more than a decade of experience in neuro-radiology, who was blinded regarding pathological findings, clinical examinations or prior radiological conclusions. Imaging analyses were performed in the following order: cMRI, DSCE-MRI and ¹H-MRS (Fig. 1).

cMRI image analysis. The cMRI image analysis (Fig. 1A-D) determined the following regions: i) Tumoral solid regions: Enhancement on contrast-enhanced T1WI or, in the case of a non-enhancing tumor, hypointensity on T1W and hyperintensity on T2WI. ii) Peritumor region: In case of a tumor that shows enhancement after contrast, the peritumor region is the area of brain parenchyma showing hyperintensity on T2W/FLAIR and hypointensity on T1WI and does not show enhancement after contrast injection; in case of a tumor that shows no enhancement after contrast, the peritumor region is the area of brain parenchyma surrounding the tumor that follows signal intensity of normal brain parenchyma. iii) The normal brain parenchyma: The contralateral NWM regions on the same slide on which solid tumoral regions were specified. iv) Tumoral cystic degeneration/necrosis regions: Significant hypointensity on T1W and hyperintensity on T2WI but no enhancement after gadolinium injection. v) Intratumoral calcification/hemorrhagic regions: Signal drop out or blooming artifacts on T2 gradient echo sequence (T2*) or post-processed susceptibility-weighted images and hyperdensity on computed tomography (if available).

Locations with signals that may interfere with the region of interest (ROI)-(signal intensity of the region of interest) or voxel placing region were excluded from further analysis (called artifact regions), including those containing tumoral cystic degeneration, calcification, hemorrhagic regions and intratumoral necrosis areas or intratumor vessels. The areas near the skull bone, subcutaneous adipose tissue and regions with significant variations in magnetic susceptibility were also excluded.

DSCE-MRI analysis. A DSCE-MRI sequence was performed during the first pass of a bolus contrast injection before contrast-enhanced T1W using dynamic T2*-weighted

gradient-recalled echo-planar imaging. The slice thickness was 5 mm, the same as for the other sequences, which assists in juxtaposing the perfusion results. The following regions were determined: i) The tumoral region: The solid area with the most hypervascular areas appearing as 'hot spots' on the CBV color map (usually coded in red), avoiding vascular territories. ii) Peritumoral regions and normal contralateral brain parenchymal region: Those identified on cMRI.

Subsequently, in the cerebral blood volume (CBV) and cerebral blood flow (CBF) maps, three ROIs (3-5 mm in diameter) were placed in the tumoral region, peritumor region and normal contralateral white matter on the same slide and location to measure CBF and CBV values for each region using the 'clone tool' and the 'copy ROI tool' in the workstation (Fig. 1E and F) to measure the same size and tumor region in each image; this is to ensure the consistency and reproducibility in ROI placement. Hemodynamic parameters were calculated from the concentration-time curves of relative CBV (rCBV) and rCBF by dividing the maximum values of the intratumor and peritumor regions by those of the cerebral NWM. The parameters obtained for further statistical analysis were the tumor rCBV (TrCBV) and rCBF (TrCBF) and peritumor rCBV (PrCBV) and rCBF (PrCBF).

¹H-MRS analysis. Spectroscopic imaging comprised a proton spectroscopy examination with 2D multi-voxel chemical shift imaging using a proton-resolved spectroscopy sequence. Spectroscopic analysis showed the level of metabolites, including Cr at 3.15-3.0 ppm, Cho at 3.36-3.21 ppm and NAA at 2.18-2.01 ppm.

The voxels were placed to encompass tumor, peritumor and NWM parenchymal regions and avoid artifact regions. ¹H-MRS imaging analysis used Cho/NAA and Cho/Cr maps to identify and quantify these regions' highest metabolite ratios. Subsequently, in the spectroscopy voxel images, placing three ROIs (3-5 mm in diameter) in the region of highest metabolite ratio of the tumoral region, peritumor region and normal contralateral white matter on the same slide (Fig. 1G-N), the 'clone tool' and the 'copy ROI tool' were used in the workstation to measure the same size and tumor region in each image; this was to ensure the consistency and reproducibility in ROI

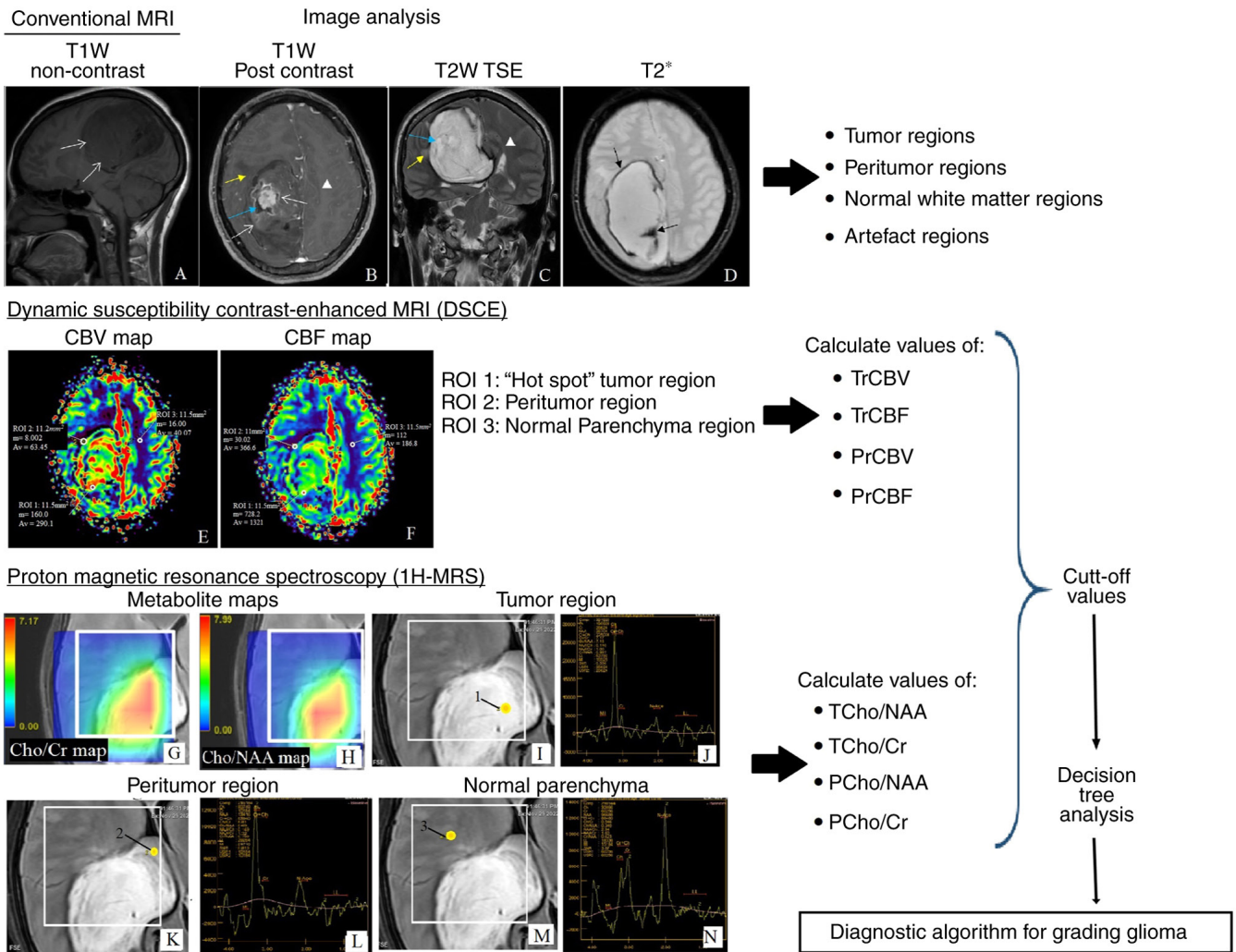


Figure 1. Research methodology flowchart. A 34-year-old female patient with a heterogenous Tumor located in the frontal-occipital-thalamus region. Imaging analyses were performed in the following order: cMRI (A-D), DSCE-MRI (E and F) and ¹H-MRS (G-N). cMRI (A) T1W non-contrast, (B) T1W post-contrast, (C) T2W TSE and (D) T2*. cMRI image analysis determined the following regions for further analysis: Tumoral solid regions (white arrows in A and B), peritumor lesion (yellow arrows in B and C) and the normal brain parenchyma of the contralateral NWM regions (white triangle in B and C). Artifact regions include tumoral cystic degeneration (blue arrows in B and C) and calcification or hemorrhagic regions (black arrows in D). In the DSCE-MRI analysis, three ROIs were placed in the tumoral region (ROI 1), peritumor region (ROI 2) and normal contralateral white matter (ROI 3) in the (E) CBV and (F) CBF maps with the 'hot spots' areas method in the tumoral region. The TrCBV, TrCBF and PrCBV and PrCBF were then calculated. In the ¹H-MRS analysis, (G) a Cho/Cr map and a (H) Cho/NAA map were used to identify and quantify these regions' highest metabolite ratios (increasing from blue to red) and ROIs (1, 2 and 3) were placed to measure ratio metabolites in tumor regions in correspondence with its (I) FLAIR image comprising TCho/Cr and TCho/NAA and (J) ratio metabolites of peritumoral regions in correspondence with its (K) FLAIR image including (L) PCho/Cr and PCho/NAA compared to the normal brain parenchyma: (M) Cho/Cr and (N) Cho/NAA. The patient underwent surgical resection with a pathological diagnosis of glioblastoma, World Health Organization grade 4. ROI, region of interest; cMRI, conventional MRI; ¹H-MRS, proton magnetic resonance spectroscopy; TrCBV, tumor relative cerebral blood volume; PrCBV, peritumor relative CBV; CBF, cerebral blood flow; Cr, creatine; NAA, N-acetyl aspartate; Cho, choline; T2*, T2 gradient echo sequence; T2W TSE, T2-weighted turbo spin-echo; DSCE, dynamic susceptibility contrast-enhanced.

placement. The ratio metabolites of Cho/Cr and Cho/NAA in tumor (TCho/Cr and TCho/NAA) and peritumoral (PCho/Cr and PCho/NAA) regions were collected for further study analysis. The workstation software automatically calculated the values by dividing the values of the metabolite in the same spectrum and they were collected for further statistical analysis (Fig. 1G-N).

Histopathological examination. All patients who underwent surgery or stereotactic biopsy with histopathology were categorized as LGG (WHO grades 1 and 2) or HGG (WHO grades 3 and 4) according to the 2021 WHO categorization for central nervous system tumors (1). Pathological diagnoses

were performed by analyzing the samples prepared from the specimens after surgery/biopsy and consensus was reached by two neuropathologists blinded to the clinical outcomes (as required by the protocol of the hospital). The research team obtained the pathological result (comprised of the type of glioma and its group, as specified in the medical record) for further analysis. The grading of gliomas is typically based on histopathological features. Main pathological features include the activity of tumor cells (such as irregular nuclei and mitosis characteristics), endothelial proliferation, nuclear atypia, intratumoral necrosis and microvascular proliferation, specified from hematoxylin & eosin-stained specimens (19). LGG are classified as WHO grade 1 or 2. These tumors

are characterized by less histopathologically aggressive features, including well-differentiated cells, slower growth rate and a less invasive nature. Examples include pilocytic astrocytomas and diffuse astrocytomas. HGG are classified as WHO grade 3 or 4 and are more malignant. They exhibit more cellular atypia, increased mitotic activity and areas of necrosis. Glioblastoma multiforme is an example of a WHO grade 4 glioma and is considered one of the most aggressive types. In addition, molecular and histopathological status was also determined, including the Ki67 index and isocitrate dehydrogenase 1 and 2 (IDH1/2) mutation status, 1p/19q chromosomal arm co-deletion, H3 K27 mutations and TP53 mutation (1). The classification of glioma groups and grades differs for each type of glioma. For instance, there are several characteristics to define oligodendrogliomas (1,20) (WHO grade 2 or 3) comprised the following: i) The cellular characteristics typically consist of round or polygonal cells with a clear or finely granular appearance, resembling the cells responsible for forming the myelin sheath in the nervous system. ii) Nuclear atypia: Grade 2 oligodendrogliomas often lack anaplastic features (brisk mitotic activity, microvascular proliferation, necrosis), grade 3 oligodendroglioma often has prominent anaplastic features (necrosis, microvascular proliferation or brisk mitotic activity; significant nuclear atypia) and ≥ 6 mitotic figures per 10 high-power fields. Oligodendrogliomas may exhibit capillary proliferation calcifications. The most common alterations that could be determined under histopathology are the loss of genetic material on chromosomes 1p and 19q (1p/19q co-deletion) with IDH1 or IDH2 mutation (both features are required for diagnosis) (1,20).

Statistical analysis. The data were statistically evaluated using SPSS (version 20.0; IBM Corp.) to determine associations between MRI imaging characteristics and pathological features and establish an image-based diagnostic algorithm to categorize glioma as LGG and HGG from advanced MRI sequences. Comparisons between variables were accomplished using the independent-samples t-test. The normality of each quantitative parameter was assessed using the Kolmogorov-Smirnov test ($n=57$). The parameters with a normal distribution ($P>0.05$) were presented as the mean \pm standard deviation (SD) and compared using Chi-square or Fisher's exact tests. The parameters with a non-normal distribution ($P<0.05$) were presented as the median with 25-75th percentiles and compared using the Mann-Whitney U-test. $P<0.05$ was considered to indicate statistical significance. A receiver operating characteristic (ROC) curve was generated to determine the optimal cutoff values for each parameter by maximizing the sum of sensitivity and specificity using the Youden Index.

Subsequently, an image-based algorithm for grading gliomas was developed using parameters found to be statistically significant in a decision tree analysis with the Chi-squared automatic interaction detection (CHAID) growing method. The CHAID growing method, first proposed by Kass (21), builds the decision tree technique that relies on the Chi-square test to specify the independent variables that interfere with the dependent variable the most and the Bonferroni test (an adjusted significance test) (22,23). The equation of Chi-square

detection used in the CHAID growing method was as follows (22):

$$x^2 = \sum \frac{(A-E)^2}{E} = \sum_{i=1}^k \frac{(A_i - E_i)^2}{E_i} = \sum_{i=1}^k \frac{(A_i - n p_i)^2}{n p_i} \quad (i=1, 2, 3, \dots, k),$$

where x^2 , is the chi-square value calculated by the actual and theoretical values, k is the number of cells in the two-dimensional classification table, A_i is the actual value of i , E_i is the expected value of i , n is the total number of samples, p_i is the expected frequency of i and E_i is $n \times p_i$.

The chi-square values of the two-dimensional table were specified separately and the significance of the P-values was juxtaposed to determine the lowest P-value for the best initial classification table. The categorical variable with the lowest P-value was used as the first-level variable of the CHAID decision tree. It was then continued to categorize the target variables to obtain the second and tertiary variables of the CHAID decision tree. The process was repeated until the P-value was greater than the set statistically significant α -value or until the classification stopped when all variables were classified; however, the probability of committing the family-wise error rate increases along with the number of statistical tests.

$$\text{Family-wise error rate} = 1 - (1 - \alpha)^n,$$

where α is the significance level for a single hypothesis test and n is the total number of tests.

The Bonferroni test was used to reduce the family-wise error rate known as false-positive, as it designed an adjustment to prevent data from incorrectly appearing statistically significant. The value obtained from this test is the misclassification risk estimate. The equation of Bonferroni's test was used in the CHAID growing method (22):

$$\alpha_{new} = \frac{\alpha_{original}}{n},$$

where $\alpha_{original}$ is the original α level and n is the total number of comparisons performed.

Subsequently, the risk estimate and the algorithm's accuracy for diagnosing LGG and HGG were calculated from the obtained image-based algorithm for grading gliomas. Finally, binary logistic regression was performed to calculate predicted values for the combined parameters in the algorithm to determine sensitivity, specificity and the area under the ROC curve (AUC).

Results

Demographic features of HGG and LGG. The present retrospective study enrolled 57 patients (29 males and 28 females; 8 pediatric patients and 49 adults), including 14 with LGG and 43 with HGG. In the LGG group, five patients had grade 1 glioma and nine had grade 2 glioma. In the HGG group, 20 patients had grade 3 glioma and 23 had grade 4 glioma. The patients' demographic characteristics, glioma locations and pathological diagnoses are summarised separately for LGG and HGG in Tables II and III. The LGG and HGG groups did not differ significantly in their sex ratio ($P=0.358$), mean age ($P=0.129$) and glioma location ($P=0.351$). The mean age in the LGG and HGG groups was 27.5 ± 15.9 and 35 ± 17.2 years, respectively.

Table II. Demographic characteristics of patients with LGG and HGG and their glioma locations.

Parameter	LGG	HGG	P-value
Sex (male/female)	9/5	20/23	0.358 ^a
Age, years (mean \pm SD)	27.5 \pm 15.9	35.0 \pm 17.2	0.129 ^b
Location			0.351 ^a
Frontal lobe	13	12	
Parietal lobe	4	2	
Temporal lobe	2	3	
Thalamus and basal ganglia	0	13	
>2 lobes/locations	3	5	

^aParameters assessed for normality using the Kolmogorov-Smirnov test with a $P > 0.05$ show that they follow a normal distribution. Therefore, they are presented as the mean \pm standard deviation and compared between groups using the chi-square test. ^bComparisons were performed using the independent-samples t-test. HGG, high-grade glioma; LGG, low-grade glioma.

Table III. Account of each type of gliomas in the study based on the corresponding pathological diagnosis according to the World Health Organization 2021 classification.

Pathological diagnosis	Grade	N (%)
Papillary glioneuronal tumor	1	1 (1.8)
Ganglioglioma	1	4 (7.0)
Fibrillary astrocytoma	2	3 (5.3)
Pilocytic astrocytoma	2	1 (1.8)
Diffuse astrocytoma	2	2 (3.5)
Oligodendroglioma	2	3 (7.0)
Diffuse astrocytoma	3	17 (27.9)
Oligodendroglioma	3	2 (3.5)
Pleomorphic xanthoastrocytoma	3	1 (1.8)
Diffuse midline glioma	4	7 (12.3)
Glioblastoma	4	16 (28.1)

DSCE-MRI in grading HGG and LGG. The DSCE-MRI parameters used to categorize glioma are listed in Table IV. The TrCBV, PrCBV, TrCBF and PrCBF were significantly higher in the HGG group than in the LGG group (all $P < 0.001$).

ROC curve analyses were used to evaluate the capacity of each DSCE-MRI parameter to distinguish between HGG and LGG (Fig. 2). Their AUC, cutoff, sensitivity, and specificity, Youden index are presented in Table V. The PrCBF had the highest diagnostic ability, followed by the TrCBV, PrCBF and TrCBV with their AUC values were 0.929, 0.927, 0.912 and 0.909, respectively.

¹H-MRS in grading HGG and LGG. The ¹H-MRS parameters used to differentiate between HGG and LGG are listed in Table VI. The TCho/NAA, TCho/Cr, PCho/NAA and PCho/Cr ratios were significantly higher in the HGG than in the LGG group (all $P < 0.001$).

Table IV. Dynamic susceptibility contrast-enhanced-MRI parameters that categorize HGG and LGG.

Parameter	LGG	HGG	P-value
TrCBV	0.6 (0.5-2.3)	6.3 (3.4-9.1)	<0.001
PrCBV	0.4 (0.3-0.7)	2.1 (1.3-3.3)	<0.001
TrCBF	0.6 (0.4-2.2)	5.0 (3.8-7.0)	<0.001
PrCBF	0.5 (0.3-0.9)	2.1 (1.3-3.3)	<0.001

The parameters assessed for normality using the Kolmogorov-Smirnov test had a $P < 0.05$ and did not follow a normal distribution. Therefore, they were presented as the median (25-75th) percentiles and variables were compared between groups using the Mann-Whitney U-test. TrCBV, ratio of tumor cerebral blood volume to contralateral NWM; PrCBV, the ratio of peritumoral CBV to contralateral NWM; TrCBF, the ratio of tumor cerebral blood flow to contralateral NWM; PrCBF, the ratio of peritumor CBF to contralateral NWM; NWM, normal white matter; HGG, high-grade glioma; LGG, low-grade glioma.

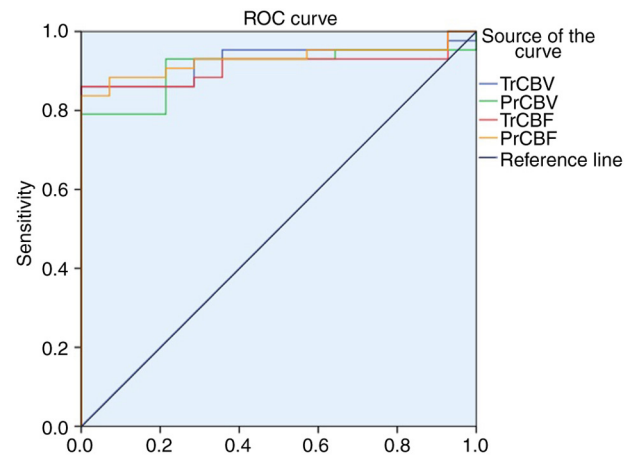


Figure 2. ROC analysis of dynamic susceptibility contrast-enhanced MRI parameters to differentiate between high- and low-grade glioma. The PrCBF (orange line) had the highest diagnostic ability, followed by the TrCBV (red line), PrCBF (green line) and TrCBV (blue line), compared to the reference line (black line). ROC, receiver operating characteristic; TrCBV, tumor relative cerebral blood volume; PrCBV, peritumor relative CBV; CBF, cerebral blood flow.

ROC curve analyses were used to determine the diagnostic ability of each ¹H-MRS parameter regarding patient classification as HGG or LGG (Fig. 3). Their related AUC, cutoff, sensitivity, specificity and Youden index are listed in Table VII. The PCho/NAA ratio had the highest diagnostic ability, followed by the PCho/Cr, TCho/NAA and TCho/Cr. Their AUC values were 0.907, 0.814, 0.791 and 0.731, respectively.

An algorithm for grading HGG and LGG based on decision tree analysis. Decision tree analysis was performed with the CHAID growing method to identify significantly different MRI parameters (Fig. 4) for inclusion in an algorithm to differentiate HGG and LGG: TrCBV, PrCBF and TCho/Cr. The algorithm's accuracy was 100% for the diagnosis of LGG and 90.7% for the diagnosis of HGG; its misclassification risk

Table V. ROC analysis of dynamic susceptibility contrast-enhanced-MRI parameters to discriminate between HGG and LGG.

Parameter	AUC	Cutoff	Sensitivity, %	Specificity, %	Youden index
PrCBV	0.909	1.25	74.4	100	0.791
TrCBF	0.912	2.79	86.0	100	0.857
TrCBV	0.927	2.48	86.0	100	0.860
PrCBF	0.929	1.26	83.7	100	0.837

AUC, area under the ROC curve; ROC, receiver operating characteristic; HGG, high-grade glioma; LGG, low-grade glioma; TrCBV, tumor relative cerebral blood volume; PrCBV, peritumor relative CBV; CBF, cerebral blood flow.

Table VI. Proton magnetic resonance spectroscopy parameters categorizing glioma.

Parameter	LGG	HGG	P-value
TCho/NAA	2.3 (1.3-4.0)	5.5 (3.2-7.9)	0.001
TCho/Cr	2.4 (1.7-3.6)	4.1 (2.8-6.4)	0.01
PCho/NAA	0.7 (0.5-1.1)	1.9 (1.4-3.0)	<0.001
PCho/Cr	1.1 (0.9-1.5)	2.3 (1.7-3.0)	<0.001

The parameters assessed for normality using the Kolmogorov-Smirnov test had a $P < 0.05$ and did not follow a normal distribution. Therefore, they were presented as the median (25-75th) percentiles and variables were compared between groups using the Mann-Whitney U-test. TCho/NAA, integral metabolite value ratio of Cho/NAA in the tumoral region; TCho/Cr, integral metabolite value ratio of Cho/Cr in the tumoral region; PCho/NAA, integral metabolite value ratio of Cho/NAA in the peritumoral region; PCho/Cr, integral metabolite value ratio of Cho/Cr in the peritumoral region; Cr, creatine; NAA, N-acetyl aspartate; Cho, choline; HGG, high-grade glioma; LGG, low-grade glioma.

estimate was 7% (Table VIII). Binary logistic regression estimated that the algorithm's predicted values for the combined parameters had a sensitivity of 88.4%, specificity of 100% and AUC of 0.940 (Table VIII).

Discussion

Gliomas are the most common intracranial tumor, characterized by diverse clinical symptoms, imaging features and prognosis. According to the 2021 WHO classification for central nervous system tumors, they are classified into four grades with increasing malignancy: LGG (grades 1 and 2) and HGG (grades 3 and 4) (1,2). The grading of tumors relies mainly on their histopathological examination after surgery or biopsy and is considered the gold standard. However, certain limitations and risks are associated with errors during the sampling procedures (e.g., small specimens or lack of neoplastic components within the malignant transformation zone and stabilization technique) and lead to inappropriate interpretation and grading and potential complications related to these procedures. While LGGs may develop slowly and remain silent over many years, HGGs have poor outcomes with more rapid progression. The standard strategy for HGG

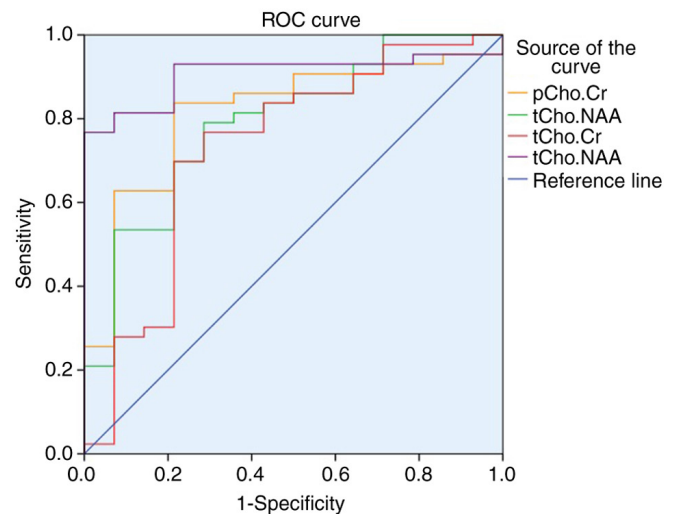


Figure 3. ROC analysis of proton magnetic resonance spectroscopy parameters to differentiate between high- and low-grade glioma. PCho/NAA (purple line) had the highest diagnostic capacity, followed by PCho/Cr (red line), TCho/NAA (green line), and TCho/Cr (orange line), compared to the reference line (blue line). ROC, receiver operating characteristic; T, tumor; Pr, peritumor; Cr, creatine; NAA, N-acetyl aspartate; Cho, choline.

treatment includes gross total resection or subtotal resection and, if available, radiotherapy and chemotherapy with temozolomide. However, these treatment methods have only prolonged the mean survival time from 2-3 weeks to 2 years (10-26%) (5,6). While recent progress in identifying genetic mutations has revolutionized management using targeted therapies for HGGs, such as recent phase 1 clinical trials focusing on *IDH1* (NADP⁺) or O-6-methylguanine-DNA methyltransferase mutations, overall advances in the biology of HGGs have not translated into significantly improved treatment protocols or survival rates (5,24,25). However, advancing radiologic diagnoses and imaging characteristics in preoperative and pre-treatment grading of gliomas would facilitate better prognosis via increased accuracy and timely diagnosis, particularly in surgical and pre- and post-operative planning for HGGs and determination of surgical target zones for LGGs (4,8).

Using cMRI with or without injection of contrast agent is particularly valuable in providing information on the anatomical structure of the brain and some feature suggest of the diagnosis of gliomas, with a diagnostic sensitivity of only 55.1-88.3% (2,6,7,9). Advanced MRI with DSCE-MRI

Table VII. ROC analysis of proton magnetic resonance spectroscopy parameters to discriminate between high- and low-grade glioma.

Parameter	AUC	Cutoff	Sensitivity, %	Specificity, %	Youden index
TCho/Cr	0.731	3.18	69.8	78.6	0.483
TCho/NAA	0.791	2.94	79.1	71.4	0.505
PCho/Cr	0.814	1.46	83.7	78.6	0.623
PCho/NAA	0.907	1.37	76.7	100	0.767

TCho/NAA, integral metabolite value ratio of Cho/NAA in the tumoral region; TCho/Cr, integral metabolite value ratio of Cho/Cr in the tumoral region; PCho/NAA, integral metabolite value ratio of Cho/NAA in the peritumoral region; PCho/Cr, integral metabolite value ratio of Cho/Cr in the peritumoral region; AUC, area under the ROC curve; ROC, receiver operating characteristic; Cr, creatine; NAA, N-acetyl aspartate; Cho, choline.

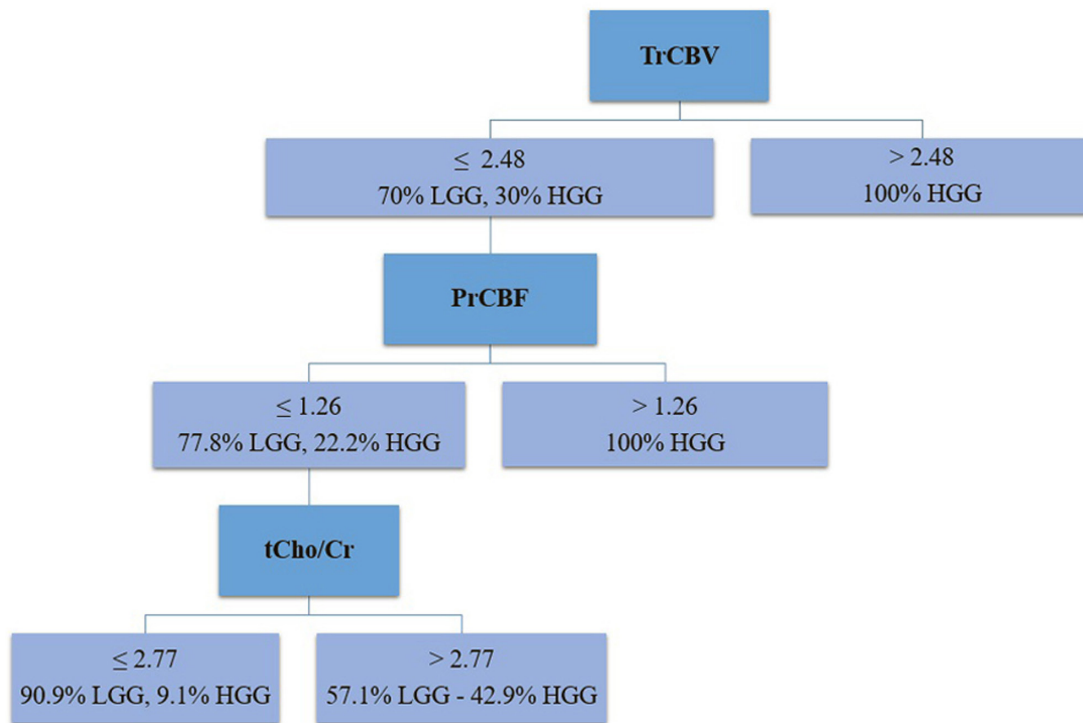


Figure 4. Algorithm for differentiating between HGG and LGG based on dynamic susceptibility contrast-enhanced MRI and proton magnetic resonance spectroscopy parameters. TrCBV, ratio of tumor cerebral blood volume to contralateral NWM; PrCBF, the ratio of tumor cerebral blood flow to contralateral NWM; NWM, normal white matter; TCho/Cr, integral metabolites value ratio of Cho/Cr in the tumoral region; HGG, high-grade glioma; LGG, low-grade glioma; Cr, creatine; Cho, choline.

and ^1H -MRS can provide additional information on tumor physiology, such as angiogenesis, metabolism, necrosis or cell density, which back up the imaging features on cMRI in assembling an accurate diagnosis, particularly in the grading of gliomas and assessing treatment response, recovery, remission or relapse (6,8,10,26). However, to date, there is no specific consensus on the cutoff thresholds for the perfusion and spectroscopy parameters used to determine cutoffs for glioma classification (14). In the present study, 57 patients with histopathologically graded gliomas (14 with LGGs and 43 with HGGs) were enrolled. The study was designed to analyze their DSCE-MRI and ^1H -MRS data from 3T MRI to evaluate the diagnostic value of various parameters (the AUC was utilized to evaluate the capacity of each parameter) and

a diagnostic algorithm for grading gliomas was constructed. Glioblastoma accounted for the highest proportion (~28.1%) of all histopathologically confirmed subjects in the present study, consistent with a previous study showing that it is the most common glioma type (13).

DSCE-MRI enables the assessment of the degree of angiogenesis, assists the differentiation between brain tumors and other non-neoplastic lesions and estimates the degree of malignancy of glioma. Previous studies have indicated a positive association between DSCE-MRI and mitotic/Ki-67 index, reflecting the tumor's malignancy grade (2,6). The degree of angiogenesis in the tumor and blood-brain barrier permeability are depicted by the color scale on the DSCE-MRI, known as 'hot-spot' areas. In the present study, the median rCBV values

Table VIII. Diagnostic algorithm for glioma grading using dynamic susceptibility contrast-enhanced magnetic resonance perfusion and proton magnetic resonance spectroscopy including tumor relative cerebral blood volume, peritumor relative cerebral blood flow and tumoral choline creatine.

AUC	Sensitivity, %	Specificity, %	Misclassification risk estimate, %	Algorithm's accuracy for LGG, %	Algorithm's accuracy for HGG, %
0.940	88.4	100	7	100	90.7

AUC, area under curve; LGG, low-grade glioma; HGG, high-grade glioma.

of the tumor and peritumor areas were lower in LGG than in HGG, with TrCBV values of 0.6 and 6.3 and PrCBV values of 0.4 and 2.1, respectively. A TrCBV cutoff of 2.48 (sensitivity=86%, specificity=100%) and a PrCBV cutoff of 1.25 (sensitivity=74.4%, specificity=100%) were used, which had AUC values of 0.929 and 0.909, respectively.

A study by Jain *et al* (27) on intracranial glioma showed that the average TrCBV values for LGG and HGG were 1.75 and 6.05, respectively, with a cutoff of 3.0 giving a sensitivity and specificity of 97.2 and 100% for grading glioma, respectively. A study by Tran *et al* (28) on 12 patients with brainstem glioma determined mean TrCBV values of LGG and HGG were 2.77 and 8.53, respectively, with a TrCBV cutoff of 3.16 giving an sensitivity of 100% and specificity of 66.7% for grading brainstem glioma, with an AUC of 0.889. A study by Chiang *et al* (25) on differentiating HGG and metastases using advanced MRI showed that HGG had a PrCBV value of $\sim 2.33 \pm 1.61$. A study by Abdel-Monem *et al* (13) on gliomas found higher TrCBV and PrCBV values for LGGs (1.16-3.50 and 0.8-2.4, respectively) than for HGGs, with cutoffs of 1.7 (sensitivity=96.9%, specificity=95.2%) and 1.0 (sensitivity=87.5%, specificity=100%), giving AUC values of 0.985 and 0.905, respectively.

The PrCBV values in the present study were similar to those in previous studies. The TrCBV values in the present study were slightly lower than the threshold values in numerous previous studies, which used a TrCBV cutoff of 3.0 (2,3,27,28). This difference may be related to the imaging protocol and technique, as well as variation in the type and number of tumors in each glioma sub-group. In addition, differences in tumor locations in previous studies may lead to differences in blood supply sources and the histological characteristics of the tumor in each territory. Nevertheless, the present study showed no difference in tumor location between HGG and LGG.

CBF provides practical information on tissue perfusion and has a strong positive correlation with rCBF (11). Previous studies have evaluated the value of rCBF in diagnosing and grading glioma. However, its results are often less reliable than rCBV results due to the appreciable variability in rCBF values across different studies (7,11,28). In the present study, the median TrCBF values with HGG and LGG were 0.6 and 5.0, respectively, with a cutoff of 2.79 (sensitivity=86%, specificity=100%). The corresponding PrCBF values were 0.5 and 2.1, respectively, with a cutoff of 1.26 (sensitivity=83.7%, specificity=100%). Tran *et al* (28) used a TrCBF cutoff of 3.56 to grade brainstem glioma, which gave an sensitivity of 83.3%, specificity of 100% and AUC of 0.917. The TrCBV and TrCBF

values were lower for glioma in the superior fossa than in the brainstem (28). Aydin *et al* (7) proposed a TrCBV cutoff of 3.25 and a TrCBF cutoff of 3.22, which gave a sensitivity and specificity of 100% for differentiating between LGG and HGG. These cutoffs are higher than those proposed by Hakyemez *et al* (11), who suggested a TrCBV cutoff of 1.98 and a TrCBF cutoff of 1.25. The appreciable variability in values among different studies may be due to differences in imaging techniques, measurement methods or inherent tumor heterogeneity, such as differences in vascularity and blood flow rates, even within different regions of the same tumor (7). Recent studies on applying rCBF with rCBV to diagnose and grade gliomas have provided relatively consistent results, suggesting a new application for rCBF in cerebral ischemia and the diagnosis and differentiation of different types of brain tumor (7,28).

Biochemical indicators in the brain can be measured using ¹H-MRS and are essential for diagnosing and differentiating benign and cancerous lesions with high specificity and sensitivity (9). The concentration of Cho-containing metabolic compounds increases with malignancy, while the concentration of normal brain cell metabolites, such as Cr and NAA, decreases (9). In the present study, the median Cho/NAA and Cho/Cr values in the tumor and peritumoral regions were lower in LGGs than in HGGs. The median TCho/NAA ratio was 2.3 in LGGs and 5.5 in HGGs, with a cutoff of 2.94 (sensitivity=79.1%, specificity=71.4%), while the median TCho/Cr ratio was 2.4 for LGGs and 4.1 for HGGs, with a cutoff of 3.18 (sensitivity=69.8%, specificity=78.6%).

Previous studies have reported inconsistent findings for ¹H-MRS parameters. The most recent research, published by Shakir *et al* (14) in 2022, indicated that the cutoff point for Cho/Cr was 3.72 (sensitivity, 83.3%; specificity, 93.7%) and that for Cho/NAA was 3.14 (sensitivity, 88.9%; specificity, 43.7%), which was close to that in the present study. Abdel-Monem *et al* (13) found a TCho/NAA value of 1.6 for LGG and 5.1 for HGG, with a cutoff of 1.0 (sensitivity, 96.9%; specificity, 76.2%) and a TCho/Cr value of 1.6 for LGG and 3.5 for HGG, with a cutoff of 1.8 (sensitivity, 100%; specificity, 76.2%), which had AUCs of 0.872 and 0.865. Verma *et al* (29) used TCho/Cr cutoffs to distinguish between LGG (<2.5), intermediate-grade glioma (2.5-4.0) and HGG (>4.0). Naser *et al* (30) reported a TCho/NAA cutoff of 1.85 (sensitivity, 74.4%; specificity, 95.8%).

In the present study, the median PCho/NAA value was 0.7 for LGG and 1.9 for HGG, with a cutoff of 1.37 (sensitivity, 76.7%; specificity, 100%), and the median PCho/Cr value was

1.1 for LGG and 2.3 for HGG, with a cutoff of 1.46 (sensitivity, 83.7%; specificity, 78.6%). Chiang *et al* (25) reported that HGGs had PCho/Cr values of 1.3 ± 0.45 for distinguishing HGGs from metastatic tumors. In the present study, higher values and thresholds than in previous studies were found for ^1H -MRS parameters, which may be explained by the use of multivoxel spectroscopy in the present study to increase spatial resolution and reduce partial volume effects. In addition, spectroscopy metabolic maps were used to locate the region with the highest concentration of metabolic compounds, including Cho/NAA and Cho/Cr maps, to enable a more specific and accurate assessment of the most active tumor metabolism region (18). By contrast, previous studies used the average ROI placement method, which would not precisely capture and locate the region with the highest abnormal metabolite concentrations. Given the heterogeneous tissue structures of glioma, particularly diffuse astrocytoma and oligodendroglioma, there may be areas of transition from low to high grades (1,9,27).

Decision trees represent the class of the most widely applied logical methods for effectively generating classifiers from data that use a tree-like structure to make decisions. The tree consists of nodes representing decision points and branches, indicating possible outcomes. The process involves recursively splitting the dataset based on input features until a particular condition is met or a predictive model is established. Numerous decision tree growing methods have been introduced nowadays; the three most common are CHAID, classification and regression tree and ID3-iterative dichotomiser (22). The CHAID growing method constructs the decision tree technique based on the Bonferroni test (an adjusted significance test) and chi-squared test to determine the independent variables that interfere with the dependent variable the most (22,23). The rationale behind CHAID is to identify significant alliances between predictor variables and the target variable by employing the chi-squared test. At each node, CHAID identifies the variable that best discriminates among different categories of the target variable, creating a split based on statistical significance. It has been widely used for the non-linear relationships among CHAID maps, which can empower predictive models with stability. The CHAID method is more optimal with categorical variables than the other growing method (22). In summary, using the CHAID growing method, decision tree analysis helps identify patterns and relationships in categorical data by recursively splitting the dataset based on the most significant variables, making it a powerful tool for classification and prediction (22,23). In the present study, determined cutoffs comprising TrCBV, PrCBF and TCho/Cr were used to categorize LGG and HGG. It may aid in achieving a 100% accurate diagnosis for LGG and 90.7% for HGG with a sensitivity of 88.4%, specificity of 100%, AUC of 0.940 and an estimated misclassification risk of ~7%. A previous study by Hasan *et al* (13) showed that combining apparent diffusion coefficient, TrCBV and TCho/NAA values using linear discriminant analysis (leave-one-out method) may achieve a diagnostic accuracy of up to 100%.

The present study had certain limitations. First, its sample size was relatively small and the research subjects in this research were assembled using a consecutive sampling method due to the shortage of the former algorithm to estimate the minimum sample size necessitated, which may affect the

representativeness of its results. Furthermore, its use of multi-voxel sequences for certain patients with glioma that were close to the bone or small may influence the concentration of metabolic compounds. In addition, adult and pediatric patients with glioma have distinctive features and their combined evaluation may have affected the research findings. Therefore, further research with a larger patient population and separate evaluation of adult and pediatric patients with glioma is necessary. Finally, this research was conducted only on DSCE-MRI and ^1H -MRS sequences without using the sequences of diffusion-weighted effects due to the widespread availability of the former two sequences on both the 3.0T and 1.5T MRI systems. When the number of patients in the DTI group is sufficient, a combined study will be carried out using a multi-modal approach of advanced MRI techniques to determine further holistic features of the glioma's characteristics.

In conclusion, the diagnostic algorithm using TrCBV, PrCBF and TCho/Cr values, which were obtained from DSCE-MRI and ^1H -MRS, increased diagnostic accuracy to 100% for LGGs and 90.7% for HGGs compared to a previous study using conventional MRI; its sensitivity and specificity fluctuate around 72.5 and 65.0%, respectively (6). This non-invasive advanced MRI diagnostic algorithm is recommended for clinical application for constructing preoperative strategies and prognosis of patients with glioma.

Acknowledgements

A part of our research has been presented at the ESNR 2023 (31) conference as a poster with the aim of receiving feedback and contributions from esteemed colleagues to enhance this study. We confirm that the content of this study was not submitted to any other journal.

Funding

No funding was received.

Availability of data and materials

The datasets generated and/or analyzed during the current study are not publicly available due to privacy concerns but are available from the corresponding author upon reasonable request.

Authors' contributions

DHiN, DHuN and MDN wrote the manuscript. DHiN, DHuN and MDN participated in the design of the study. DHiN, DHuN and MDN were involved in the acquisition of data. DHiN, DHuN, MDN, TDL, HKN and VANT participated in the analysis and interpretation of data. DHiN, DHuN and MDN confirm the authenticity of all the raw data. All authors have read and approved the final manuscript.

Ethics approval and consent to participate

The institutional review board of Hanoi Medical University (Hanoi, Vietnam) supported this retrospective study (ref. 827/GCN-HDDNCYSH-DHYHN/dated 28/03/2023). Viet

Duc Hospital's IRB automatically agreed with the other IRB (ref. 827/GCN-HDDDNCYSH-DHYHN/dated 28/03/2023). This study was conducted according to the ethical standards of the 1964 Declaration of Helsinki and its later amendments. The requirement for informed consent was waived.

Patient consent for publication

Not applicable.

Competing interests

The authors declare that they have no competing interests.

References

- Louis DN, Perry A, Wesseling P, Brat DJ, Cree IA, Figarella-Branger D, Hawkins C, Ng HK, Pfister SM, Reifenberger G, *et al*: The 2021 WHO classification of tumors of the central nervous system: A summary. *Neuro Oncol* 23: 1231-1251, 2021.
- Aprile I, Giovannelli G, Fiaschini P, Muti M, Kouleridou A and Caputo N: High- and low-grade glioma differentiation: The role of percentage signal recovery evaluation in MR dynamic susceptibility contrast imaging. *Radiol Med* 120: 967-974, 2015.
- Aprile I, Tornì C, Fiaschini P and Muti M: High-grade cerebral glioma characterization: Usefulness of MR spectroscopy and perfusion imaging associated evaluation. *Neuroradiol J* 25: 57-66, 2012.
- Riche M, Amelot A, Peyre M, Capelle L, Carpentier A and Mathon B: Complications after frame-based stereotactic brain biopsy: A systematic review. *Neurosurg Rev* 44: 301-307, 2021.
- Stupp R, Mason WP, van den Bent MJ, Weller M, Fisher B, Taphoorn MJB, Belanger K, Brandes AA, Marosi C, Bogdahn U, *et al*: Radiotherapy plus concomitant and adjuvant temozolomide for glioblastoma. *N Engl J Med* 352: 987-996, 2005.
- Law M, Yang S, Wang H, Babb JS, Johnson G, Cha S, Knopp EA and Zagzag D: Glioma grading: Sensitivity, specificity, and predictive values of perfusion MR imaging and proton MR spectroscopic imaging compared with conventional MR imaging. *AJNR Am J Neuroradiol* 24: 1989-1998, 2003.
- Aydin S, Fatihoğlu E, Koşar PN and Ergün E: Perfusion and permeability MRI in glioma grading. *Egypt J Radiol Nucl Med* 51: 2, 2020.
- Zidan S, Tantawy HI and Makia MA: High grade gliomas: The role of dynamic contrast-enhanced susceptibility-weighted perfusion MRI and proton MR spectroscopic imaging in differentiating grade III from grade IV. *Egypt J Radiol Nucl Med* 47: 1565-1573, 2016.
- Rafique Z, Awan MW, Iqbal S, Usmani NN, Kamal MM, Arshad W, Ahmad M, Mumtaz H, Ahmad S and Hasan M: Diagnostic accuracy of magnetic resonance spectroscopy in predicting the grade of glioma keeping histopathology as the gold standard. *Cureus* 14: e22056, 2022.
- Majós C, Aguilera C, Alonso J, Julià-Sapé M, Castañer S, Sánchez JJ, Samitier A, León A, Rovira A and Arús C: Proton MR spectroscopy improves discrimination between tumor and pseudotumoral lesion in solid brain masses. *AJNR Am J Neuroradiol* 30: 544-551, 2009.
- Hakyemez B, Erdogan C, Ercan I, Ergin N, Uysal S and Atahan S: High-grade and low-grade gliomas: Differentiation by using perfusion MR imaging. *Clin Radiol* 60: 493-502, 2005.
- Abe T, Mizobuchi Y, Nakajima K, Otomi Y, Irahara S, Obama Y, Majigsuren M, Khashbat D, Kageji T, Nagahiro S and Harada M: Diagnosis of brain tumors using dynamic contrast-enhanced perfusion imaging with a short acquisition time. *Springerplus* 4: 88, 2015.
- Hasan AMS, Hasan AK, Megally HI, Khallaf M and Haseib A: The combined role of MR spectroscopy and perfusion imaging in preoperative differentiation between high- and low-grade gliomas. *Egypt J Radiol Nucl Med* 50: 72, 2019.
- Shakir TM, Fengli L, Chenguang G, Chen N, Zhang M and Shaohui M: 1H-MR spectroscopy in grading of cerebral glioma: A new view point, MRS image quality assessment. *Acta Radiol Open* 11: 20584601221077068, 2022.
- Yamasaki F, Kurisu K, Satoh K, Arita K, Sugiyama K, Ohtaki M, Takaba J, Tominaga A, Hanaya R, Yoshioka H, *et al*: Apparent diffusion coefficient of human brain tumors at MR imaging. *Radiology* 235: 985-991, 2005.
- Sener RN: Diffusion MRI: Apparent diffusion coefficient (ADC) values in the normal brain and a classification of brain disorders based on ADC values. *Comput Med Imaging Graph* 25: 299-326, 2001.
- Huisman TAGM: Diffusion-weighted and diffusion tensor imaging of the brain, made easy. *Cancer Imaging* 10 (1A): S163-S171, 2010.
- Hangel G, Schmitz-Abecassis B, Sollmann N, Pinto J, Arzanforoosh F, Barkhof F, Booth T, Calvo-Imirizaldu M, Cassia G, Chmelik M, *et al*: Advanced MR techniques for preoperative glioma characterization: Part 2. *J Magn Reson Imaging* 57: 1676-1695, 2023.
- Louis DN, Ohgaki H, Wiestler OD, Cavenee WK, Burger PC, Jouvet A, Scheithauer BW and Kleihues P: The 2007 WHO classification of tumours of the central nervous system. *Acta Neuropathol* 114: 97-109, 2007.
- Giannini C, Scheithauer BW, Weaver AL, Burger PC, Kros JM, Mork S, Graeber MB, Bauserman S, Buckner JC, Burton J, *et al*: Oligodendrogliomas: Reproducibility and prognostic value of histologic diagnosis and grading. *J Neuropathol Exp Neurol* 60: 248-262, 2001.
- Kass GV: An exploratory technique for investigating large quantities of categorical data. *J Royal Stat Soc C (Applied Statistics)* 29: 119-127, 1980.
- Yang Y, Yi F, Deng C and Sun G: Performance analysis of the CHAID algorithm for accuracy. *Mathematics* 11: 2558, 2023.
- Milanovic M and Stamenkovic M: CHAID decision tree: Methodological frame and application. *Econ Themes* 54: 563-586, 2016.
- Weller M, Stupp R, Hegi M and Wick W: Individualized targeted therapy for glioblastoma: Fact or fiction? *Cancer J* 18: 40-44, 2012.
- Chiang IC, Kuo YT, Lu CY, Yeung KW, Lin WC, Sheu FO and Liu GC: Distinction between high-grade gliomas and solitary metastases using peritumoral 3-T magnetic resonance spectroscopy, diffusion, and perfusion imagings. *Neuroradiology* 46: 619-627, 2004.
- Henriksen OM, Hansen AE, Muhic A, Marner L, Madsen K, Møller S, Hasselbalch B, Lundemann MJ, Scheie D, Skjøth-Rasmussen J, *et al*: Diagnostic yield of simultaneous dynamic contrast-enhanced magnetic resonance perfusion measurements and [¹⁸F]FET PET in patients with suspected recurrent anaplastic astrocytoma and glioblastoma. *Eur J Nucl Med Mol Imaging* 49: 4677-4691, 2022.
- Jain KK, Sahoo P, Tyagi R, Mehta A, Patir R, Vaishya S, Prakash N, Vasudev N and Gupta RK: Prospective glioma grading using single-dose dynamic contrast-enhanced perfusion MRI. *Clin Radiol* 70: 1128-1135, 2015.
- Tran D, Nguyen DH, Nguyen HK, Nguyen-Thanh VA, Dong-Van H and Nguyen MD: Diagnostic performance of MRI perfusion and spectroscopy for brainstem glioma grading. *Eur Rev Med Pharmacol Sci* 26: 7938-7948, 2022.
- Verma A, Kumar I, Verma N, Aggarwal P and Ojha R: Magnetic resonance spectroscopy-revisiting the biochemical and molecular milieu of brain tumors. *BBA Clin* 5: 170-178, 2016.
- Naser RKA, Hassan AAK, Shabana AM and Omar NN: Role of magnetic resonance spectroscopy in grading of primary brain tumors. *Egypt J Radiol Nucl Med* 47: 577-584, 2016.
- No authors listed: ESNR 2023. *Neuroradiology* 65 (Suppl 1): S1-S146, 2023.



Copyright © 2024 Nguyen et al. This work is licensed under a Creative Commons Attribution-NonCommercial-NoDerivatives 4.0 International (CC BY-NC-ND 4.0) License.